Thermomechanical characterization of high-speed train braking materials to improve models: Numerical validation via a comparison with an experimental braking test

R. Mann, V. Magnier, J.F. Brunel, P. Dufrénoy, M. Henrion, E. Guillet-Revol

Thermomechanical characterization of high-speed train braking materials to improve models: numerical validation via a comparison with an experimental braking test

R. Mann [1], V. Magnier[1*], J.F. Brunel[1], P. Dufrénoy [1], M. Henrion[2], E. Guillet-Revol[2]

[1] *Univ. Lille, CNRS, Centrale Lille, UMR 9013 - LaMcube - Laboratoire de Mécanique, Multiphysique, Multiéchelle, F-59000 Lille, France*
[2] *Flertex, FRANCE*

Abstract

Today, the development of brake pads is carried out by empirical feedback validated by experimental bench tests. Nevertheless, these test campaigns are time-consuming, costly and ultimately do not help to understand phenomena for improving performances (coefficient of friction, durability, noise, etc.). To overcome these limitations, numerical braking models have been developed for several years. They need to be representative of the experimental reality in order to predict the current performance of brake systems and ultimately improve them. The difficulties, especially for high energy dissipation applications such as high-speed train (HST) braking systems, lie in the fact that thermomechanical coupling is important to consider, which particularly affects the behaviour of brake linings. According to the literature, this thermomechanical evolution is not sufficiently taken into account. In this work, a complete methodology is proposed for the identification of the behaviour of friction materials under coupled mechanical and thermal loads. In a second step, the properties obtained are injected into a simulation of a real and representative braking system. An experimental test with enriched instrumentation on a HST braking system con-

*Corresponding author. Tel: +33 (0)3 28 76 73 57; fax: +33 (0)3 28 76 73 61
E-mail address: vincent.magnier@polytech-lille.fr

figuration is separately conducted. A comparison between numerical and experimental results is carried out to validate the complete approach. Finally, based on the good results provided by the model, an optimization on the brake pas design is proposed, which allows a better distribution of the thermo-mechanical sollicitations and wear reduction.
Keywords: Experimental/numerical comparison; Thermomechanical characterization of friction pad; Thermomechanics simulation; full-scale rail brake test bench

1. Introduction

With the constant increase in maximum speed in the field of transportation, new developments in braking devices have been required to ensure braking performance and passenger safety. These developments consist in improving the geometry and materials of the braking components to limit, among other things, thermal localizations and excessive wear of the components.

In the railway sector, thermal localizations consist of hot bands or hot spots that can be observed during braking by infrared measurements and friction recordings ([1]). These phenomena occur especially during high energy thermal braking where the temperature can reach at the contact more than 1000^oC. These thermal gradients lead to a non-homogeneous temperature field, which can lead to a degradation in braking performance ([2]) or an increase in brake pad wear ([3]). In addition, they can reduce the lifetime of the braking system in the event of thermal cracking ([4]) or fading ([5]).

To limit severe thermal localizations, brake pads must be flexible enough to adapt to the geometry of the disc and rigid enough to make the contact surface as large as possible. These conditions must be respected regardless of the temperature level reached. To get this compromise, the solution is to work on both the design and the materials that make up the friction pad.

Today, the development of new brake pads is mainly based on industrial feedback with iteration on a real test bench (scale 1) in order to meet braking

requirements in terms of performance and endurance. The high cost and duration of these tests imply moving towards an alternative path such as numerical models to target relevant parameters for better designing (shape, choice of material properties, etc.).

Indeed, in order to reduce the number of experimental tests necessary to improve brake pads, the numerical approach can quickly lead to the choice of the new configuration using, for example, the finite element method (FEA). Recently, Kao et al.[6] have developed a three-dimensional FE model capable of performing a coupled thermomechanical analysis. The authors study the effect of wear on the distribution of contact pressure. They used this model to study hot judders in a disc brake. Such models provide information on the disc average temperature reached during braking assuming a uniform distribution of the heat flow along the circumferential direction and lead to an explanation of the hot bands by a movable and variable contact area of the pad in the radial direction [7]. Abubakar and Ouyang ([8]) simulated brake pad wear using commercial FEA software and compared their results to an associated automotive brake system. All numerical models show that the evolution of the distribution of contact pressure, due to thermal expansion, wear and heating of system components, is an important parameter to explain the occurrence of thermal localizations during braking ([9]).

To take these phenomena into account in numerical simulations, the contact pressures between the disc and the pads are often determined and updated by the thermomechanical model, mainly at the beginning of braking. Due to the context of strong non-linearity and competition between the different mechanisms, this step requires a significant amount of computation time to converge. In [7] the impact of the mechanical and thermal properties of the pad sintered material, used for high energy braking such as HST, has been widely studied and has demonstrated its importance in the face of the propensity of thermal localizations development. However most previous and current studies use a model of linear elastic mechanical behaviour of the pad friction material without temperature dependence [7, 10, 11, 12, 13, 14]. The properties come from

characterizations established from a virgin sample (extracted after manufacture), and do not take into account the temporal evolution of mechanical or thermal properties despite the extreme level of loading encountered during certain braking sequences.

Thus, in this paper, the objective is to propose a complete approach from the thermomechanical characterization of the friction material to the proposal of a new design to reduce thermal localizations. As a first step, a complete thermomechanical characterization is performed on laboratory tests (variable temperature compressive tests, laserflash and dilatometry). For the thermomechanical compressive test, a non-contact method (digital image correlation) is used. Such characterization has already been done in [15] by considering influence of mechanical load level at room temperature. A loading history effect is shown, corresponding to the occurence of material damage at given levels of mechanical loads. This characterization is extended here in temperature and a constitutive law is proposed. The identified behaviour is an elasto-plastic model as a function of temperature. Then, material properties are implemented into a FEA model of the braking system for a thermomechanical braking simulation. Then the numerical results are compared to experimental ones for a HST braking on a real scale dynamometer. This comparison is done using enhanced thermal instrumentation (Infrared camera and thermocouples). Result validate the model and the proposed strategy. Finally, based on the results, brake pad design is proposed that allows a better heat distribution at the contact.

2. Thermomechanical characterization of the friction pad material

2.1. Thermomechanical compressive tests

A compressive test (broadly representative of brake lining loading in service) is developed. An originality of the protocol set up is the use of digital image correlation (DIC) [16, 17, 18] within an oven. The DIC provides both local (deformation mechanism etc.) and global (macroscopic behaviour) information on the material. Moreover, by judiciously choosing the moments of image ac-

quisition, the elastic and the residual behaviours can be identified.

Concerning the material, a sintered material is used for railway applications. It is based on an industrial formulation of an existing sintered material and its overall composition is given in the table 1.

Components	Weight %
Metallic matrix	70
Graphite	20
Ceramic	10

Table 1: Sintered material basic composition

This material is obtained by compacting component powders before sintering at high temperature (below the melting temperature of the components).

At room temperature, this material has already been characterized in [15] and a loading history effect on mechanical properties was noted.

An extension of these test is performed in a high temperature furnace as shown in figure 1. The force sensor is located at the end of the upper column, which measures the load applied to the sample. To avoid damaging the force sensor, a cold water circulation cooling system has been designed and introduced. The displacement fields are determined using the Yadics image correlation software [YADICS] which has the particularity of focusing on recording images in the same modality.

The details of the instrumentation inside the furnace are specified in figure 2. For the compressive test, the dimensions of the sample were chosen to be greater than the representative volume element. Therefore, after a few tests, cubic samples of $20mm$ is choosen. A particular attention is paid to the parallelism of the

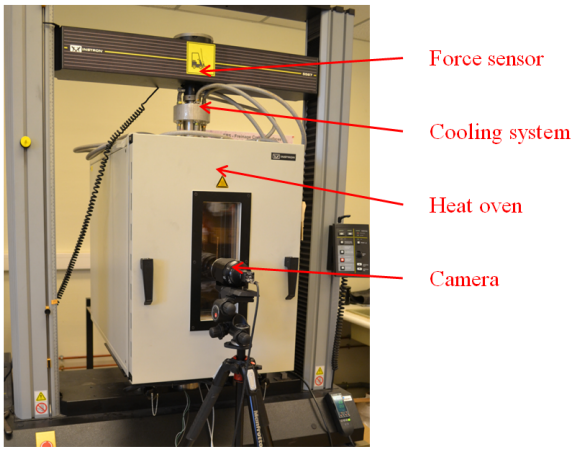

Figure 1: General view of the developed system: closed oven with the camera.

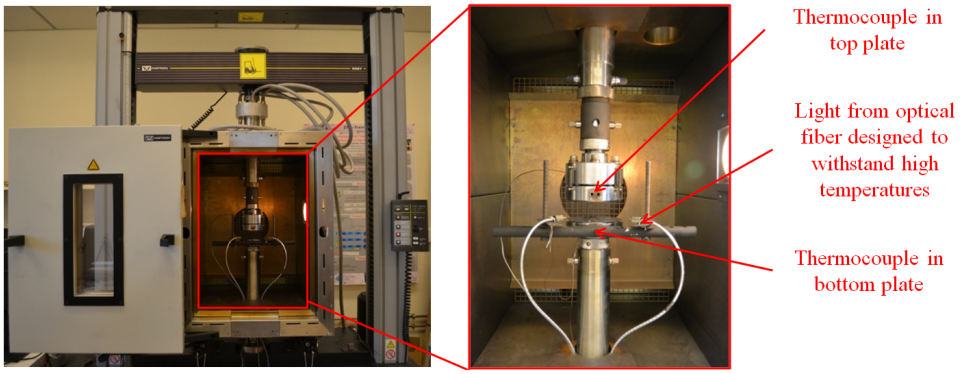

Figure 2: Interior view of the furnace and additional bench instruments.

sample faces as well as the parallelism of the trays of the compression machine. To carry out the DIC, a surface was previously uniformly painted black with high temperature paint. Then on this surface, a speckle, essential for correlation, was obtained using a high temperature stable spray paint (900^oC). The results
105 are shown in figure 3. The characteristic size of the speckle is satisfactory because it is lower than the resolution of the camera ($1\ pixel\ =\ 7\ \mu m$ determined according to the area of the surface, the focal length and the lens used). The

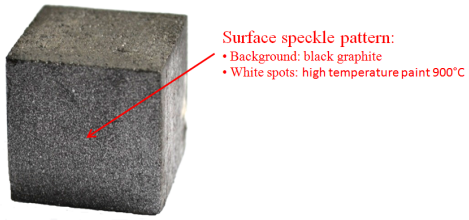

Figure 3: Surface speckle pattern adapted to high temperatures.

deformation rate is set at 0.01 mm/s for each load level tested. Each preload and maximum charge level is kept out of the loading and unloading stages for 4 seconds. The test is performed at 480^oC according to the protocol presented in table 2.

Level number	1	2	3	4	5	6	7	8	9	10	11	12	13
Preload (MPa)	1	1	1	1	1	1	1	1	1	1	1	1	1
Load level (MPa)	3	4	5	6	7	8	9	10	11	12	13	14	15

Table 2: Test procedure established for compressive test

2.1.1. Results: Unloading strain fields

Throughout the compressive test protocol, pictures are taken at different times. In order to determine both the elastic behaviour (between a green star and a red one in figure 4) and the residual behaviour (between a red star and a black one in figure 4). More precisely on the elastic part, it has been shown in [15] that at room temperature, there is neither relaxation nor creep (correlation established between a green and a yellow star on each load step). Nevertheless, for the high-temperature test, the elastic behaviour seems more complex. This elastic discharge will be referred latter to a "secant elastic modulus".

In the compression test at room temperature, the results on the strain field show "bands" of uniform strains. These results have already been noted in [15] where a link with the microstructure was shown to be particularly related to the

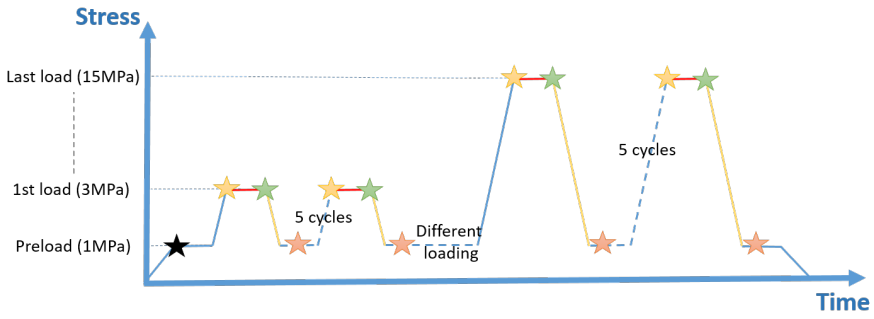

Figure 4: Explanation of pictures used in DIC to extract the results.

presence of graphite particles which are softer compared to the matrix. These strain bands develop and eventually group together according to the level of loading. From the point of view of the associated mechanisms, this translates into matrix damage in areas of high graphite concentration.

In the high-temperature compression test, the same phenomena occur. Nevertheless, these strain bands seem to be more numerous and more extensive.

From a quantitative point of view in terms of average value over the whole sample, it appears that the elastic behaviour for the two tests is equivalent along the compression axis whatever the load level. The values are shown on each thumbnail in figure 5. As an example for the 15MPa test, the average strain obtained for the test at ambient temperature is 0.36% while it is 0.37% for the test at high temperature.

In terms of global results (figure 6), the high-temperature compression test shows a lower evolution of the elastic modulus than the other test but remains in the same order of magnitude. Concerning the evolution as a function of the load level, thermal test exhibits a more constant evolution compared to the one at room temperature with lower damage effect. It also appears that the behaviour converges towards a value of elastic modulus equal to 3700MPa which can be due to the prevalence of the metallic matrix behavior, little affected at this temperature level.

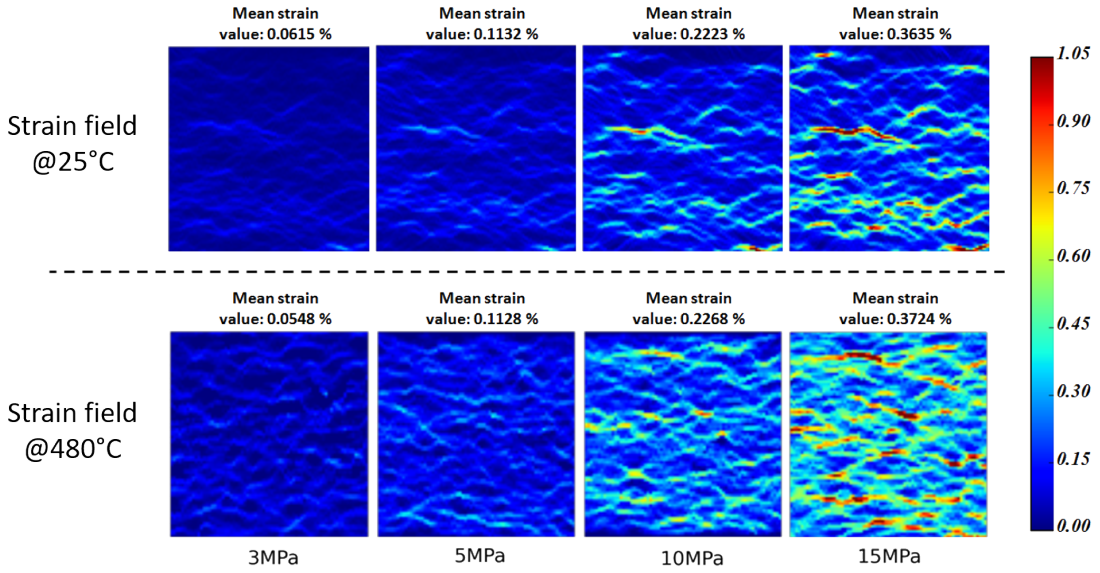

Figure 5: Unloading vertical strain fields - Same scale.

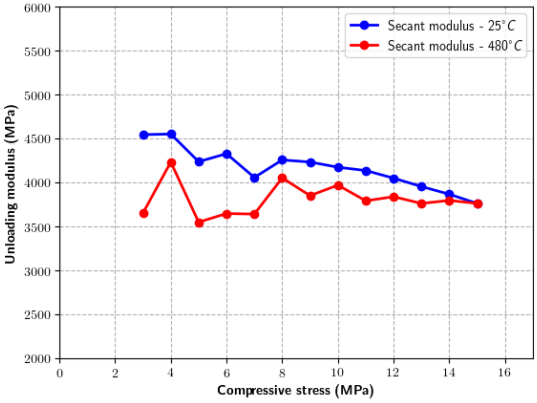

Figure 6: Evolution of the secant modulus (during unloading) with load level for two temperatures ($25°C$ and $480°C$) for the pristin sintered material.

2.1.2. Results: Residual strain fields

The residual strains at the two temperature levels are presented in figure 7 with the same scale. For both temperature tests, the strain bands are super-

imposed on those obtained on the elastic behaviour. More precisely, the plastic stress is located in the matrix, especially in areas where graphite particles are close together.

In terms of quantitative information, the average residual deformation values are reported for the two temperature tests in figure 8. The curves show a larger evolution of residual strains at 480^oC than at 20^oC. In addition, for the hot compression test, above 5 MPa, the average residual deformation value is higher than the elastic deformation. For example, at 15 MPa, the average residual deformation value is twice as high as the deformation at the unloading. This can be explained by a collapse of the mechanical properties of copper and iron, which form the matrix of the sintered material. With increasing temperatures, the plastic behaviour of the sintered material has a major influence compared to the elastic behaviour. In order to establish a first model, the yield strength of the sintered material is identified at 5 MPa at room temperature and at 3 MPa at high temperature. A strain-hardening modulus was determined using the least squares method, resulting in 3457 MPa for the room temperature test and 1450 MPa at 480 ^oC.

To determine and complete the framework for the behaviour of the sintered material, the stress-strain curves of the tests performed at 25^oC (with blue curves) and 480^oC (with red curves) are presented in figure 9. The curves correspond to the total deformations obtained at the end of each charge level (connected by a dotted line) obtained by the DIC technique. For each test, the continuous line corresponds to the load of the last cycle at 15 MPa. From the previous results and those of the last loading/unloading of the figure 9, several comments can be established on the behaviour of the sintered material at temperature:

- The elastic range decreases with temperature (from 5 to 3 MPa with a temperature increase from 25^oC to 480^oC),
- An elastic-plastic behaviour is observed, the hardening increases with tem-

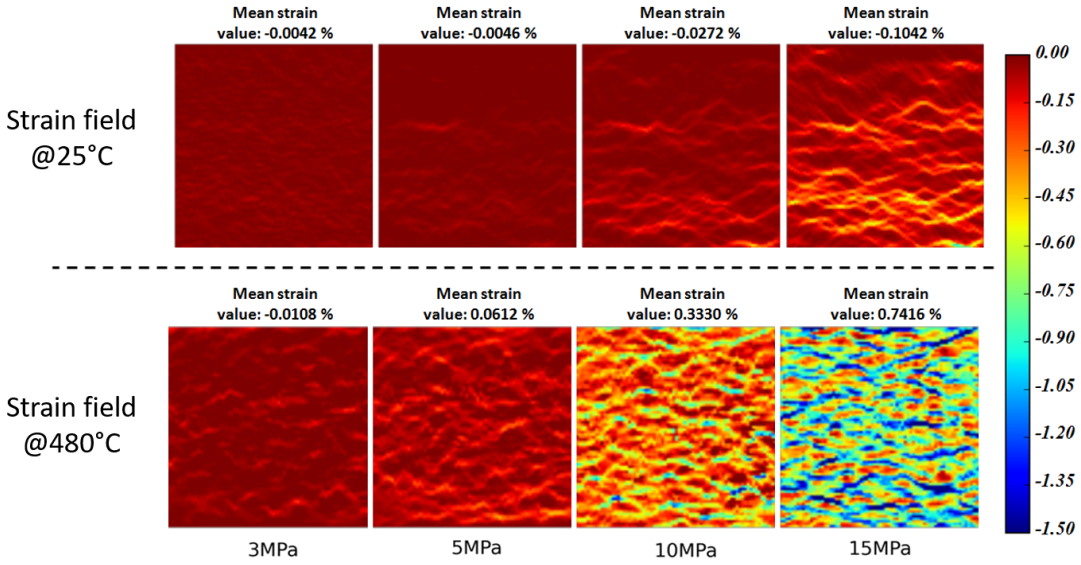

Figure 7: Absolute residual strain fields obtained for some load levels with the virgin material at different temperature ranges - Same scale.

perature,

- The elastic behaviour decreases with the load for each temperature test,
- Non-linearity is observed during unloading, indicating dissipative behaviour, which increases as the load increases (this observation is not shown here). This dissipation can be associated with non-linear effects of the material: non-cohesion of the particles with the matrix, dissipation of graphite particles, porosity effects, etc.

2.2. Thermal characterizations of the friction pad material

The thermal properties are characterized by experimental tests in the initial virgin state of the sintered materials. Thermal conductivity λ and the heat volume capacity $\rho.C_p$ were determined by the Laser Flash Analysis (LFA) technique up to 600^oC and under nitrogen atmosphere to avoid degradation by oxidation of the components. The LFA technique is based on the measurement

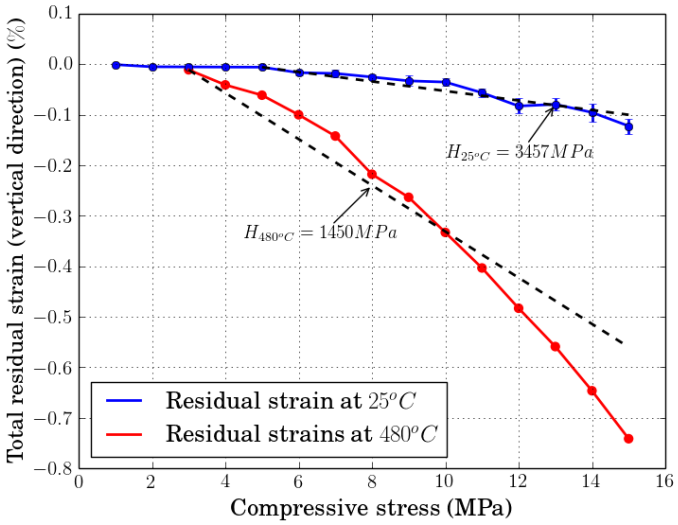

Figure 8: Evolution of the mean absolute residual strain in vertical direction in function of the pressure and temperature ranges.

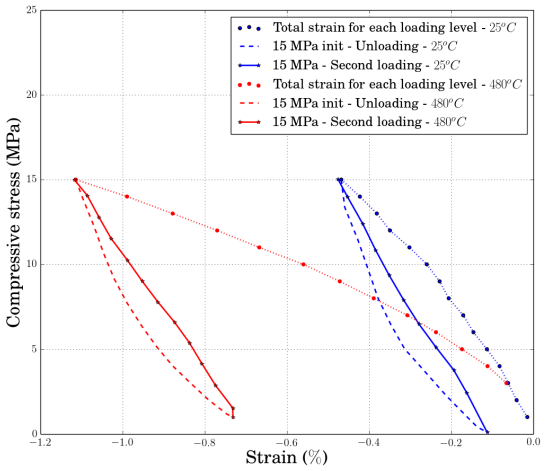

Figure 9: Stress-strain curves of the sintered material at two temperatures ($25°C$ and $480°C$) obtained from DIC technique.

of the transient temperature of the rear surface of a sample when a pulsed laser illuminates the front. This technique avoids interference between the thermal sensor and the heat source [20].

Five samples of the sintered material were extracted in the same pad in the normal direction from the surface of the brake pad. They were tested with the same test procedure to assess the reproducibility of the results. The sample extraction plan is presented in the figure 10.

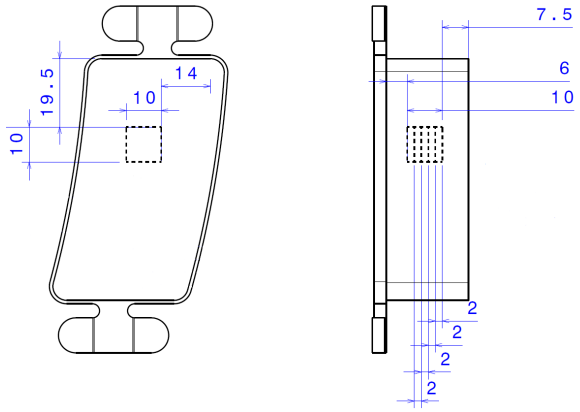

Figure 10: Extraction of samples in sintered brake pads to characterize thermal properties.

As shown in the figure 11, the thermal properties of the sintered material change with temperature. The error bars added in the graphs confirm the good reproducibility of the tests with a low dispersion of the results obtained.

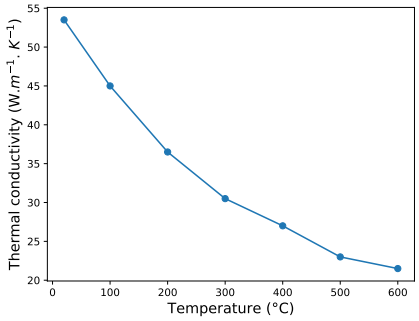

(a) Thermal conductivity

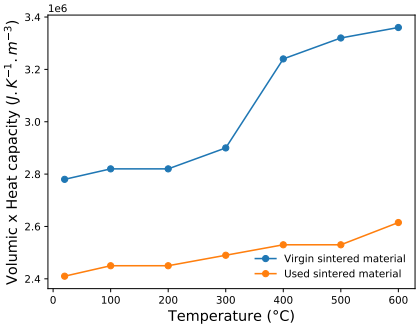

(b) Heat volume capacity

Figure 11: Thermal conductivity (a) and the heat volume capacity $\rho.C_p$ (b) obtained for the sintered material by the laser flash technique.

For the thermal expansion, a rectangular sample was extracted with the dimensions: $5 \times 5 \times 5\ mm^3$. The test is performed up to 300^oC in nitrogen atmosphere with 3 cycles. The results of the mean value are presented in Figure 12. This average evolution is used in the numerical models.

In order to take into account all the information extracted from the previous experimental tests, a user material subroutine (UMAT) is developed in the

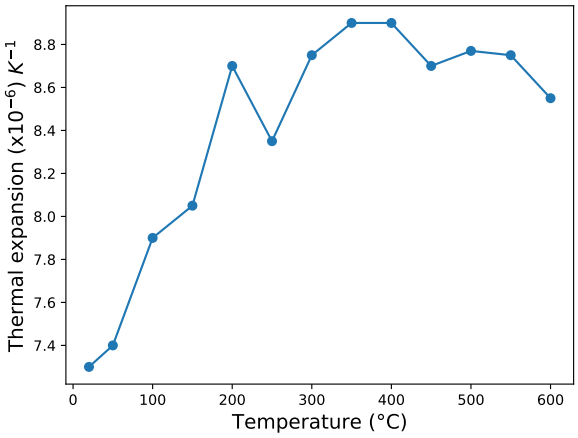

Figure 12: Experimental characterization of the thermal expansion coefficient of the sintered material under nitrogen ambiance.

FEA ANSYS software [Ansys]. The mechanical model of the sintered material considered is an elastic-plastic model with damage. A linear interpolation of mechanical and thermal properties is established between the temperature ranges of 25^oC and 480^oC. For temperatures above the maximum characterization temperature (480^oC), the properties included in the UMAT are the properties identified at 480^oC. This subroutine is based on the radial return mapping developed by Simo and Hughes [22].

2.3. Mechanical and thermal characterization of the disc

The behavior model and properties of the other parts composing the brake system are presented in figure 13.

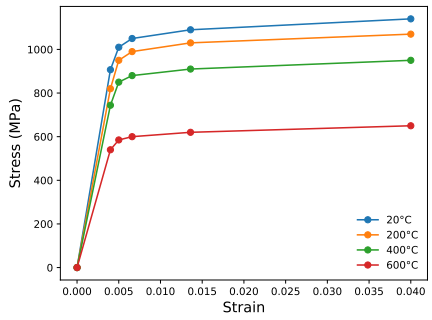

(a) Law of behaviour at different temperatures

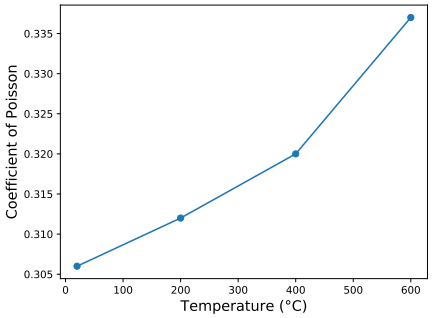

(b) Coefficient of Poisson

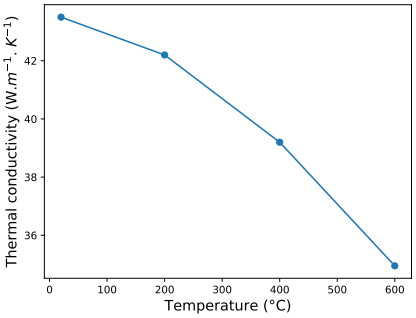

(c) Thermal conductivity

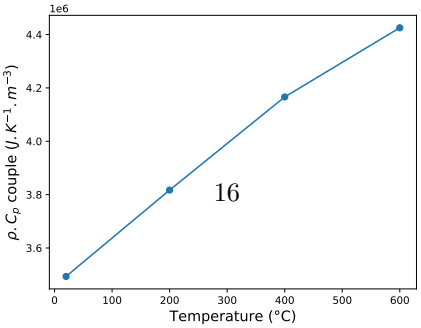

(d) Heat volume capacity

From the point of view of mechanical behaviour as a function of temperature, a classical behaviour of a steel with an elasto-plastic type evolution has been found. The yield strength decreases as a function of temperature starting from a value of 1000 MPa for the test at 20^oc and ending at 540MPa for the test at 600^oc.

This behavior has also been implemented in a UMAT as previously done for the sintered material.

3. Experimental data: Tests on a inertia dynamometer (HST configuration)

An experimental campaign on sintered brake pads was carried out on Flertex's full-scale rail brake test bench. This campaign was carried out on the basis of an adapted UIC-type programme defined by the International Union of Railways [UIC]. The configuration (wheel, caliper, lining etc.) is that of a HST brake disc.

3.1. Brief description of the bench and instrumentation

The full description of the tests as well as the instrumentation is described in detail in [15]. In a few words, 79 brake strokes were performed with different speeds (ranging from 80kph to 320kph), different loads (ranging from 10 to 36 kN), different inertias (from 5 to 7 tons) and different types of braking (dry brake, wet brake, drag brake). Measurements on the weight and height of the linings were taken 6 times in order to estimate a law of wear evolution. Two brake pads are used, acting again both sides. The pad is made of 10 pins which are all instrumented with one thermocouple located at 12mm depth from the contact surface. On the pad facing the front face of the disc, other thermocouples are placed at a depth of 6mm (except pins n^o 1 and n^o 6, the number of each pin is shown in the figure 15). On the disc surfaces, 3 rubbing thermocouples are located on 3 different radii. An infrared camera is also used to obtain the

luminance on the disc and thermal gradient indications. Based on the experimental protocol, the first high energy dissipation braking test is n^o 55. In [15], it was shown that this test n^o 55 severely degraded the material. Therefore, prior to this specific braking test, the loading was not high enough to significantly change the material's behaviour in depth. It is therefore reasonable to consider before test 55 that the material is virgin with temperature-dependant properties. These properties can be deduced from the compression characterization test performed in section 2.1.

The numerical model, which will be described in section 4 only considers hot bands. Thus, in order to compare the numerical results with those of the experimental, the selection of the experimental braking is based on infrared thermographies which must have the same kind of thermal locations. The selection of the braking n^o 26 seems to be a good candidate. This braking has an initial speed of 200 km/h, a total load of 10000 N and a mass of 5 tons.

3.2. Experimental results of the braking n^o 26

3.2.1. Standard test bench acquisitions

Figure 14 shows the different results obtained with the standard instrumentation of the brake test n^o26.

The average coefficient of friction obtained is stable during braking at a value of 0.38, the braking time is 130 s, the maximum pressure is obtained after a delay of 4 seconds and the observed loss of speed can be considered as constant during the contact phase. The results of the three rubbing thermocouples (inner(InR), mean(MR) and outer(OR) radii of the disc) on the front face (FF) as well as the 3 thermocouples on the back face (BF) are presented for the front and rear surfaces. An average of these six thermocouples is added to figure 14 with the notation "TC_MEAN". The results show a higher temperature on the median radii on both surfaces of the disc.

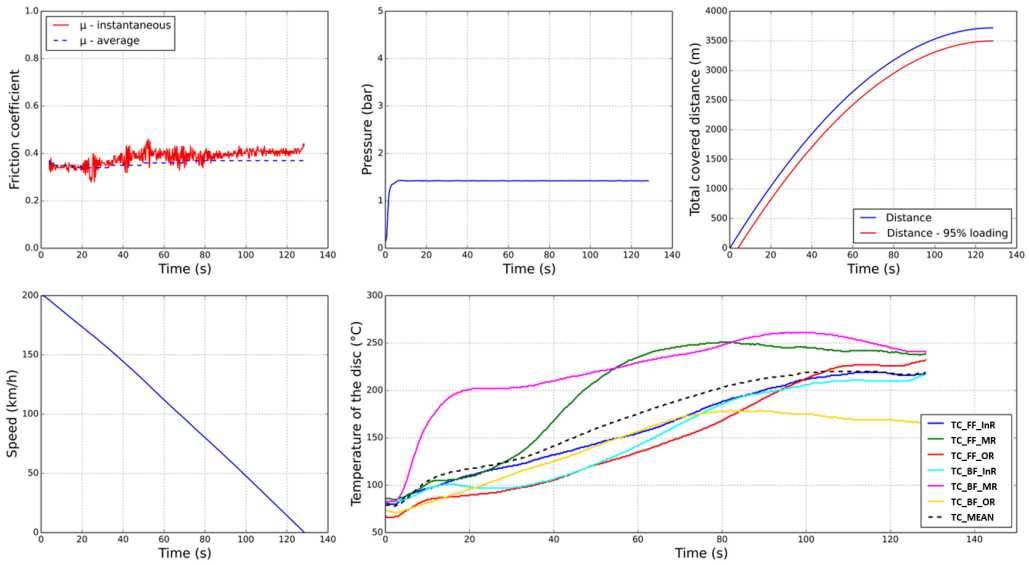

Figure 14: Standard instrumentation results for the braking 26. Rubbing thermocouples are located on the front face (FF) and back face (BF).

3.2.2. Brake pad thermocouples results

The responses of the 18 thermocouples located into the pads during braking n^o 26 are shown in figure 15 for the front face and in figure 16 for the rear face. The figures show a lower temperature in the middle of the pad (pin n^o 4 and n^o 9) which can be explained by the application of normal load that is not uniform at the back of the plate due to the dovetail (no force transmitted in the middle of the backplate). The highest temperature is measured at the leading edge of the pad on both sides (especially on the pin n^o1) due to the engagement effect with rotation.

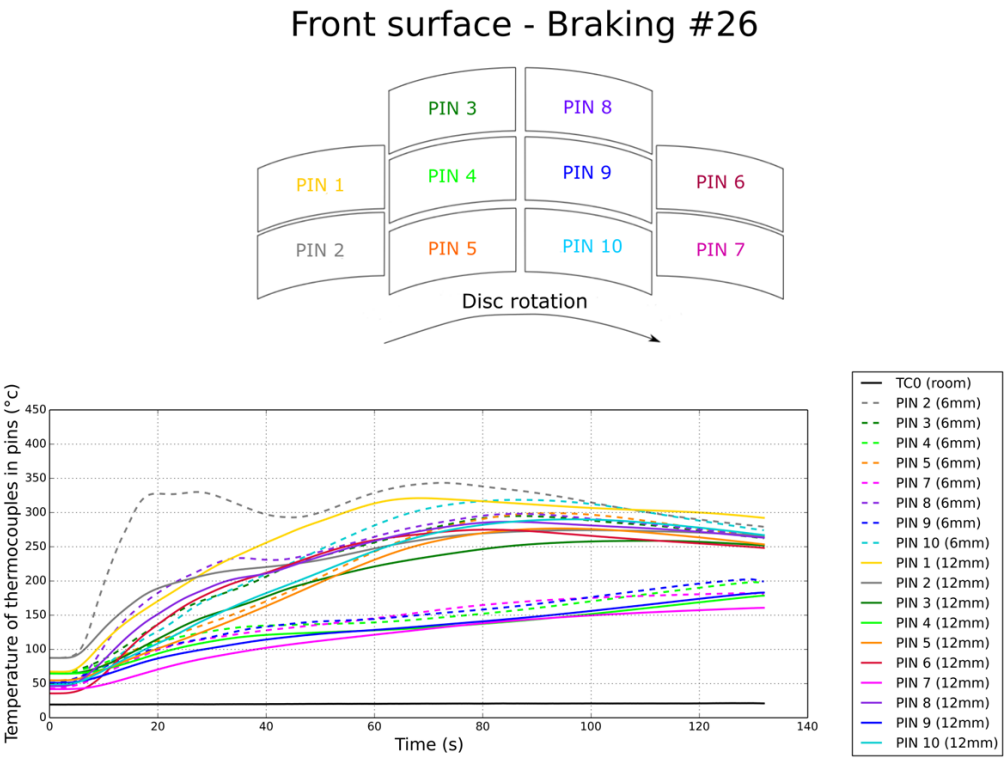

Figure 15: Thermocouples acquisitions for each pin during braking n^o26 - FRONT FACE.

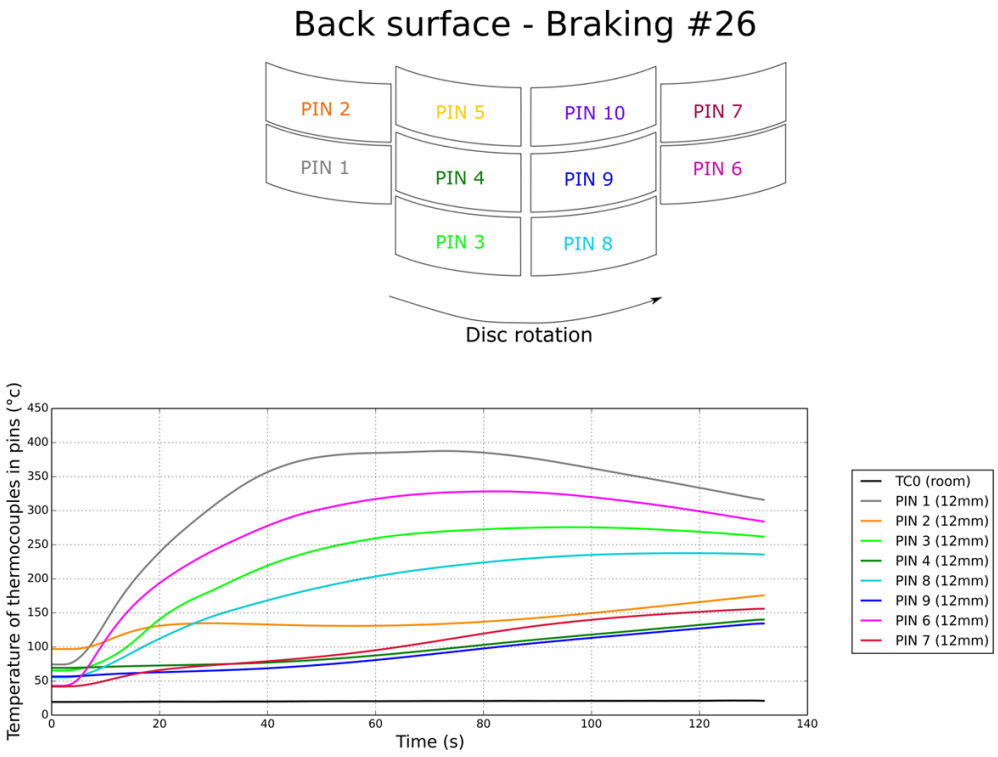

Figure 16: Thermocouples acquisitions for each pin during braking n^o26 - BACK FACE.

3.2.3. Infrared thermographs

To study the thermal localizations observed on the front face of the disc, infrared thermographs during braking n^o 26 are shown in figure 17. The results alongthe braking are presented with the same scale in terms of luminance corresponding to the accumulation of the radiated heat flux. No correction of emissivity is made and it is considered uniform. Observing the results of the IR, thermal localizations in the front surface of the disc appear with two hot bands located at the inner and outer radii of the disc. The hot bands push until they coalesce in the middle of the disc. These results are consistent with the thermocouple data presented in figures 14 (rubbing thermocouples) and 15 (thermocouples inserted in the pins), i.e. the pin n^o2 near the inner radius has

a high heating rate at the beginning of braking, followed by a more uniform heating until the end.

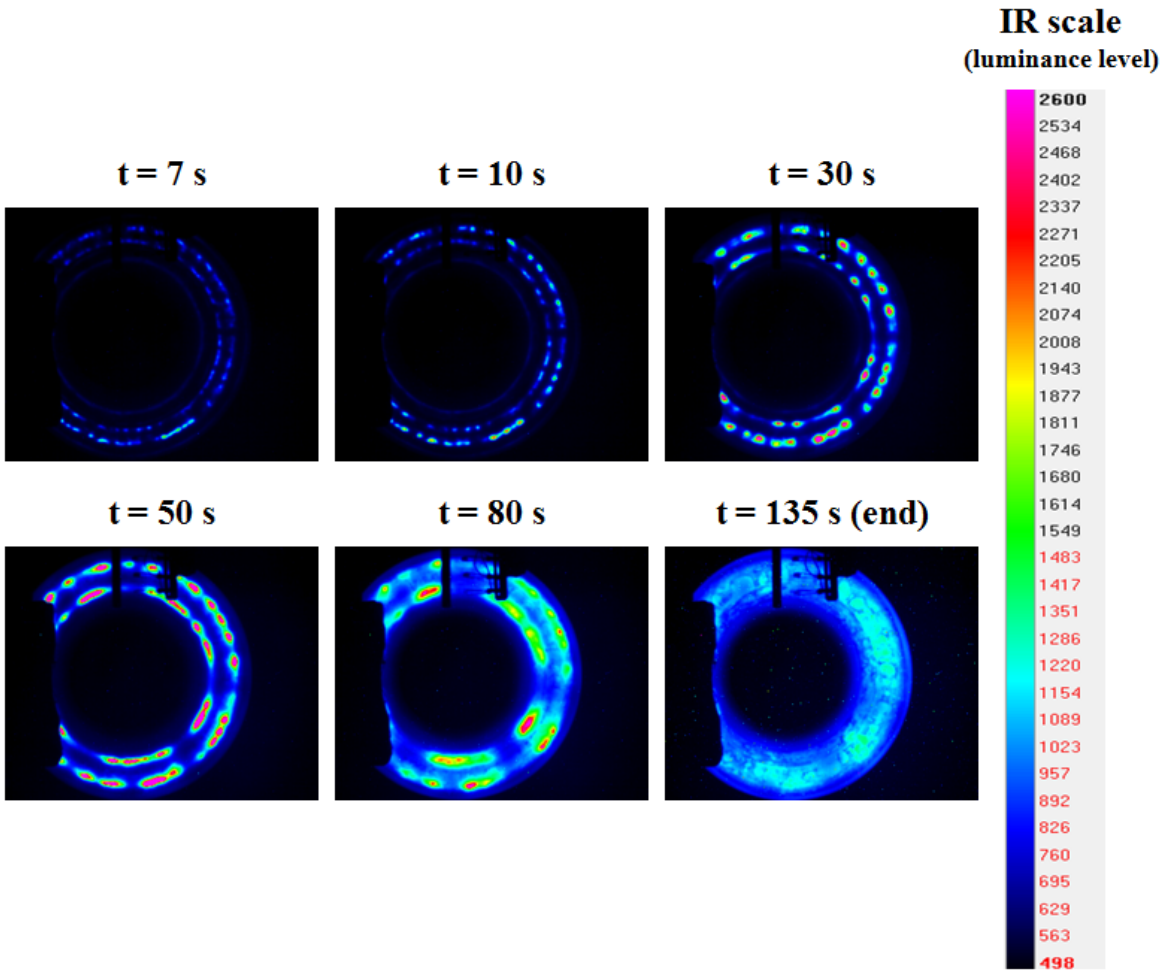

Figure 17: Infrared thermographies of the disc along the braking n^o26 displayed with the same scale in terms of luminance (uniform emissivity).

The experimental data obtained from the braking sequence are valuable information to compare with the numerical model.

4. Braking simulation results related to experimental data

The hypothesis made in this work is to neglect the angular thermal gradient due to the discontinuous contact between the disc and the brake pads. Only a gradient along the radius of the disc is taken into account, which leads to hot bands. About the sequence of the numerical calculation (figure 18), the first step is to determine the initial contact pressure between the disc and the brake pads. The total heat flux resulting from this contact is determined using the relationship :

$$\Phi = \mu(V) * F * V \tag{1}$$

where μ is the friction coefficient, V is the sliding speed, and F the normal force applied to brake pads.

310

The heat partition between the disc and the pad is obtained by the Vernotte model [24] assuming a perfect contact between semi-infinite solids according to the proportionality of their effusivities (ξ_i). In the case of short braking, the pads and disc can be considered as semi-infinite solids. The assumption of perfect contact requires that the average temperatures of the two contact surfaces are similar. It does not take into account the interface layer due to wear debris. These assumptions lead to a single parameter model for the thermal problem with a heat partition coefficient, α, corresponding to the proportion of the total heat Φ assigned to the disk. Its value is determined according to the effusivities and surfaces in contact:

$$\alpha = \frac{S_{Disc} * \xi_{Disc}}{S_{Disc} * \xi_{Disc} + S_{Pad} * \xi_{Pad}} \tag{2}$$

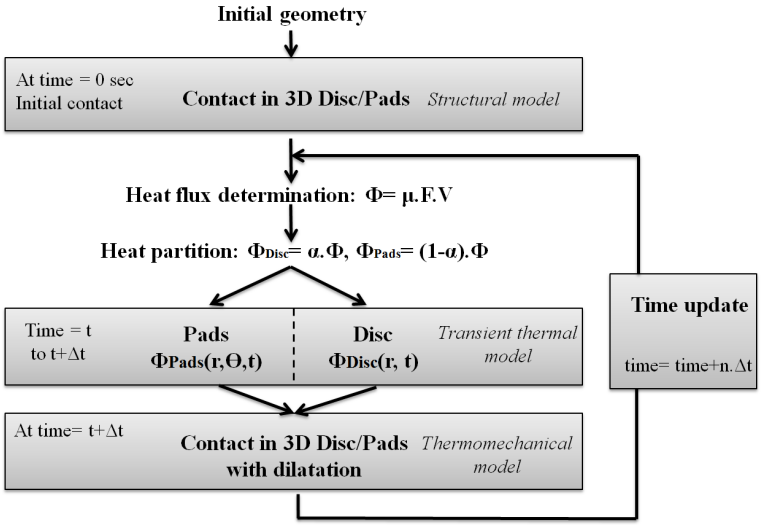

Figure 18: Architecture of the braking model

A decoupled thermomechanical resolution is performed. More precisely, a transient thermal analysis is done. The computed temperature fields are injected into the mechanical model. A thermomechanical resolution is performed, giving deformations of the disc and brake pads due to the thermal expansion leading to an update of the contact pressure distribution. This cycle is carried out iteratively until the end of braking, allowing regular updating of contact pressures.

4.1. Boundary conditions of the 3D braking model

The main boundary conditions applied on the thermomechanical brake system are illustrated in Figure 19 and can be summarized as:

- The inner radius of the hub is fixed and the base surface of the hub is fixed along the Y direction,
- A rotation condition of the disc in the counterclockwise direction is applied to obtain the engaging effect and sliding status in the contact disc/pads,

- The caliper extremities are fixed corresponding to the attachment points of the experimental setup, a load distributed on 4 nodes is applied corresponding to the braking load,
- The displacement of pad holders and dovetails are coupled in X and Z directions.

For the thermomechanical model of the setting giving the disc profiles due to thermal expansion, it looks like the axisymmetric model presented in Figure 20 without the heat flux. The temperatures obtained for the disc and hub nodes and extracted from the thermal analysis are just input into the thermomechanical model to obtain the dilatation of the components and the corresponding disc profile.

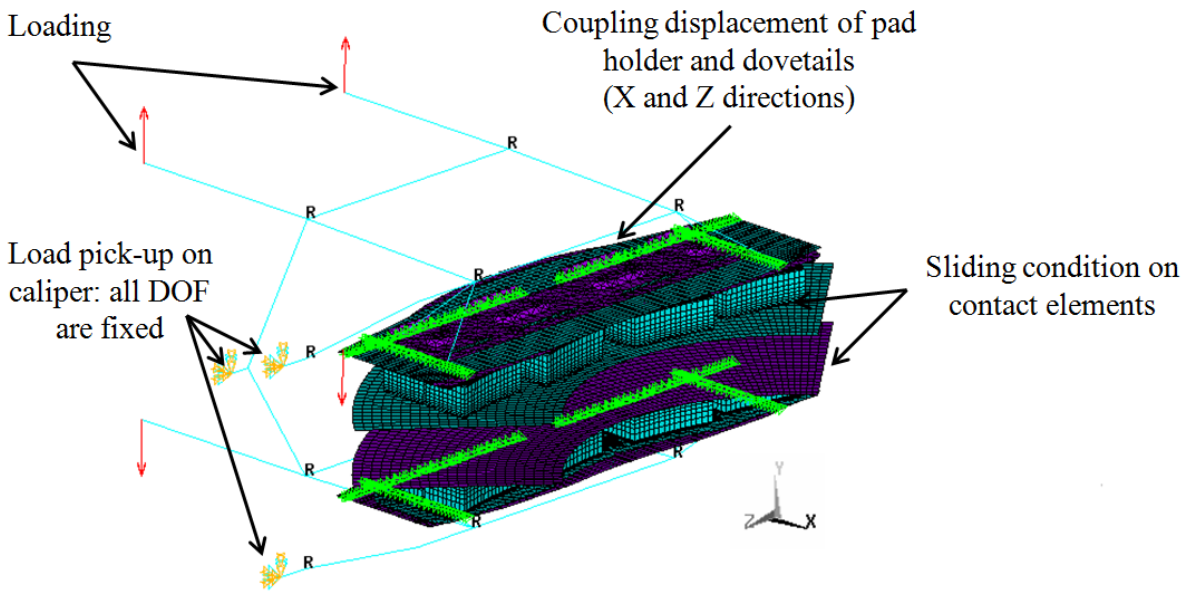

Figure 19: Boundary conditions applied to the thermomechanical 3D model including brake pads.

Concerning the thermal analysis, the boundary conditions are reported in

figure 20 for the disc and hub, and Figure 21 for the brake pads. The thermal model of the disc and hub is axisymmetric, and a 3D thermal model for the brake pads. Both models include heat flux determined from radial pressures obtained in the thermomechanical model including brake pads (Fig. 19).

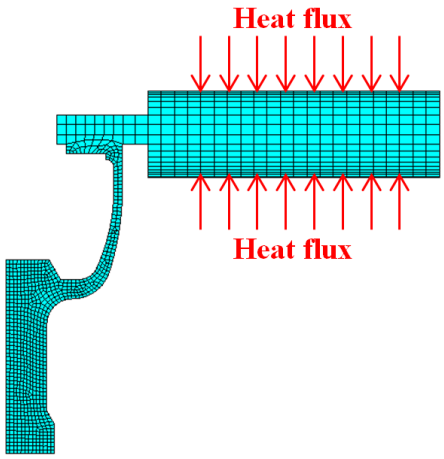

Figure 20: Thermal boundary conditions applied to the disc.

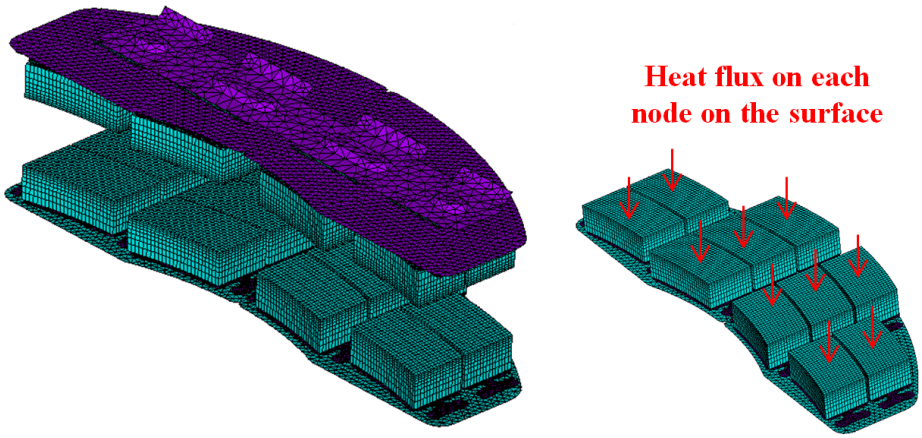

Figure 21: Thermal boundary conditions applied to the brake pads.

The disc deformations resulting from the thermal expansion in the 3D model are considered axisymmetric, like the model shown in figure 20 (without the heat flow but with the temperatures resulting from the thermal resolution). The contact between the disc and pads (both faces) is performed using penalty method contact algorithm with a control of the maximum penetration during simulation (maximum 3 μm).

In order to take into account wear of sintered material into braking simulations, an Archard model has been considered [25]. A corresponding energy wear law varying with temperature which has been identified from the weight loss measurement during bench tests (Fig. 22).

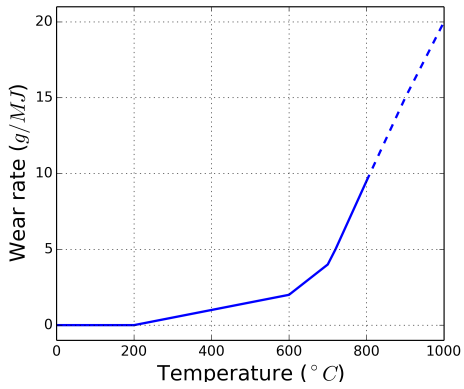

Figure 22: Wear model used in the simulation.

For each brake simulation cycle, the energy accumulated from the heat flux is determined for all nodes of the brake pad contact surface. Using the Archard model, the change in positioning height is determined by the relationship :

$$\Delta h_{node} = \frac{W_{node} \cdot E_{node}}{S_{node}} \tag{3}$$

where Δh_{node} is the positioning change in height, W_{node} the wear coefficient obtained from the wear law in function of the node temperature, E_{node} the energy

accumulated in the node, S_{node} the surface around the node.

4.2. Braking parameters and initial conditions

As presented previously, the selected braking to simulate is the braking n^o26. Thus, the braking parameters are:

- an initial speed of 200 *kph*,
- a total load of 10000 N applied at the extremities of the caliper,
- a mass to stop of 5 *tons*.

Based on the kinetic energy and power encountered, the braking duration was estimated at 130 sec as obtained with the experimental test. Inspired from the braking results n^o26 shown in Figure 14, a constant friction coefficient value of 0.38 is used to determine the generated heat flux. During the experimental tests, four seconds were set to obtain the maximum load with the caliper. A total of 24 contact pressure updates were performed, including 4 during the increase in the mechanical load of the caliper. A uniform initial temperature of 45^o is required for all brake components except the disc and pads. Indeed, due to the brake start condition presented in the test sequence, a homogeneous disc and hub temperature is considered at 80^oC. In addition, as shown in figures 15 and 16, the pin temperatures are not similar and the initial homogeneous temperatures of the experimental results are taken into account in the numerical simulation. No convection is applied during braking simulations due to its low impact during a short braking and because the disc is not ventilated. The mechanical and thermal properties of the pad sintered material and the disc steel are taken into account as a function of pressure and temperature using the user material subroutine (UMAT) developed for the FE ANSYS software [Ansys] with the values presented in the previous section 2.1.1.

4.3. Comparison of the modeling braking results related to the experimental data

In this section, the main braking results obtained with the simulation are presented to be compared with the experimental data obtained during bench tests.

4.3.1. Presentation of the main numerical results of the braking simulation

Figure 23 shows the main numerical results of the simulation. The contact pressure at the front panel interface and the thermal results of the disc and brake pads are presented at three moments: when the applied load is at its maximum, when the observed temperature is at its maximum and at the end of braking.

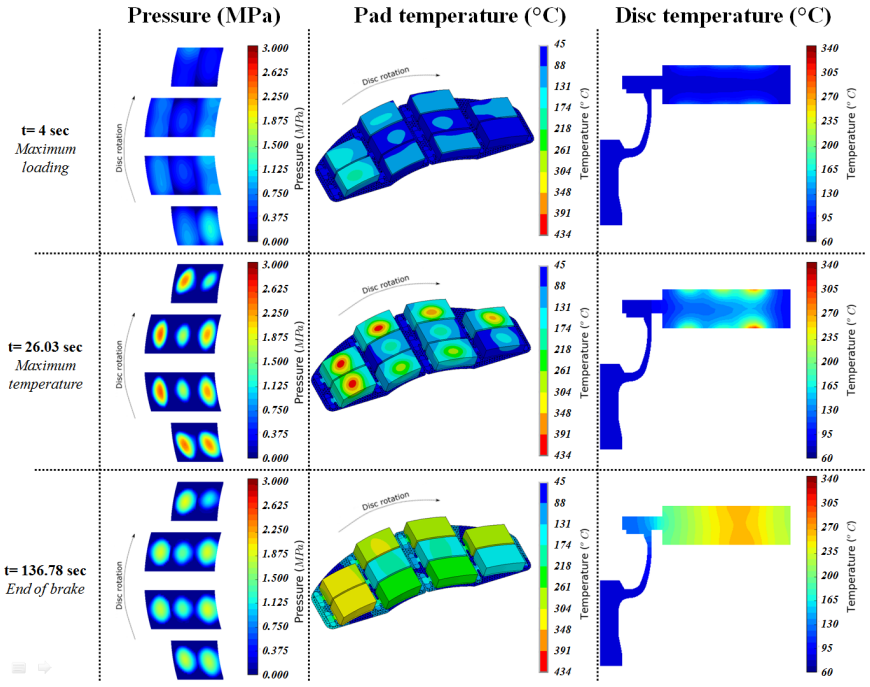

Figure 23: Contact pressure at the interface (MPa) and temperature results of the disc and brake pads along the braking n^o26.

The contact pressure between the disc and the front brake pad show a non-uniform distribution of contact along the braking path. The contact pressure is

higher for the pads located at the leading edge, which is due to the rotation of the disc. The pins located at the inner and outer radii with a maximum value of 3 MPa also have a high pressure. This non-uniform distribution is generally due to the non-uniform application of the load behind the brake pads transmitted by the pad holder in the HST application (Fig. 19) and the rigidity of the brake pads (design, materials, etc.).

From this non-uniform pressure distribution, the generated heat flow is injected into the thermal models of the brake pads and disc. Thus, a non-uniform temperature distribution is observed on the pins, as the contact pressure. A maximum temperature of 434^oC is obtained at the time $t =$ 26.03 *sec.* The thermal results of the disc illustrate three thermal locations in bands shape observed at the inner, medium and outer radii. During braking, they develop to achieve complete in-depth heating. Similar results were obtained at the front and rear surface of the disc. These results are compared with the experimental data in the following section.

4.3.2. Comparison of the temperature at the front disc surface

First, a comparison of the thermal localizations is performed between the numerical and experimental results on the front surface of the disc. The thermal results on the disc from the model (lower part of each thumbnail) are compared in figure 24 with those obtained by thermography (upper part of each thumbnail). The results are reported temporally (t=4s, 10s, 30s, 50s, 80s and 135s)through 6 thumbnails. On each thumbnail, the experimental results show the face of the disc while the numerical results are presented via an axisymmetric section to visualize the heat diffusion in depth.

To facilitate the comparison of results, three location boxes, in purple in figure 24, are identified in the IR acquisitions and are reported in the numerical results of the disc for each thumbnail. As can be seen, braking begins with three thermal bands. These localizations increase during braking. Nevertheless, in the middle of the contact and on the outer radius (purple boxes in the middle and right), the localization is more intense. After a while, a coalescence of the

two hot bands appears (t>80s) for both experimental and numerical results. In conclusion, it appears that qualitatively the results show similarities on thermal localization between experimental and numerical results.

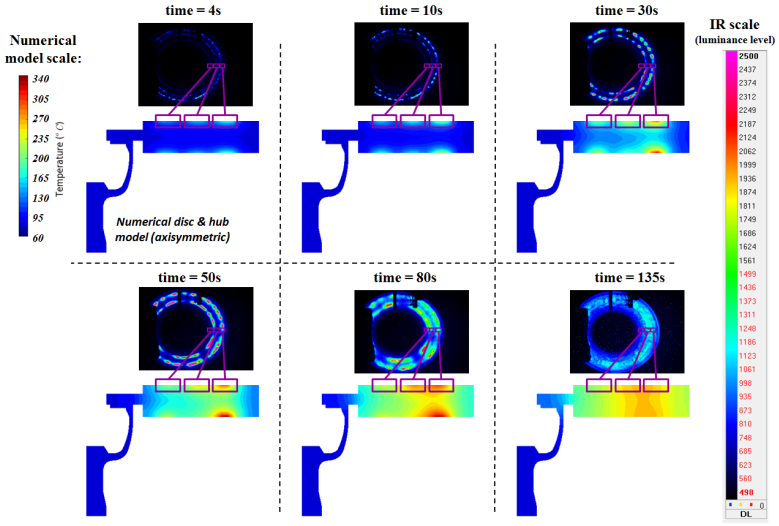

Figure 24: Comparison of thermal localizations observed by thermograph acquisitions (displayed at the same scale in luminance with a uniform emissivity) with thermal simulation results of the disc (axisymmetric representation).

Due to the unknown variation of in emissivity during braking, no quantitative temperature information was extracted from the IR acquisitions. However, this information can be extracted from the friction thermocouples located along the different radii (200, 250 and 300mm) at the front and back surfaces of the disc. To compare the temperature on the disc surface, some nodes were selected on the model. This selection is presented the figure 25 (on the left) for the front and rear surfaces and corresponds to the experimental locations of the rubbing thermocouples. On the right side of the figure, the thermal evolution is reported from the model (top figure) and from the rubbing thermocouples (bottom figure). The colour code, indicating the position of each thermocouple, is kept on both figures. The dotted curve represents the average of the temperatures

obtained.

It appears that the trends are similar both on the evolution of each curve and on the values. A higher temperature is observed for thermocouples located on the average radius of the disc. These localizations correspond to the thermal ones shown in figure 25.

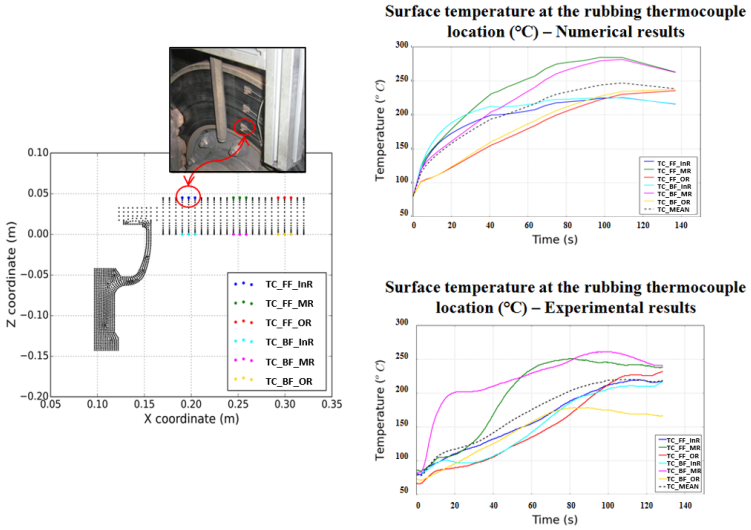

Figure 25: Illustration of the selected nodes to determine the surface temperature corresponding to rubbing thermocouple location, and comparison between numerical and experimental results.

4.3.3. Comparison of the temperature into the brake pins

For the comparison between numerical/experimental results of the brake pad temperature, a selection of nodes corresponding to the locations of the experimental thermocouples in the model is performed (figure 26). Selections are made at both depths: 6 mm and 12 mm from the initial surfaces (shown in the figure26 for braking n^o2). It should be noted that wear is considered which modifies the thickness of the pads. The wear model is inspired from the

Archard's law with coefficients identified from thickness measurements along the braking sequence (sequence interruptions).

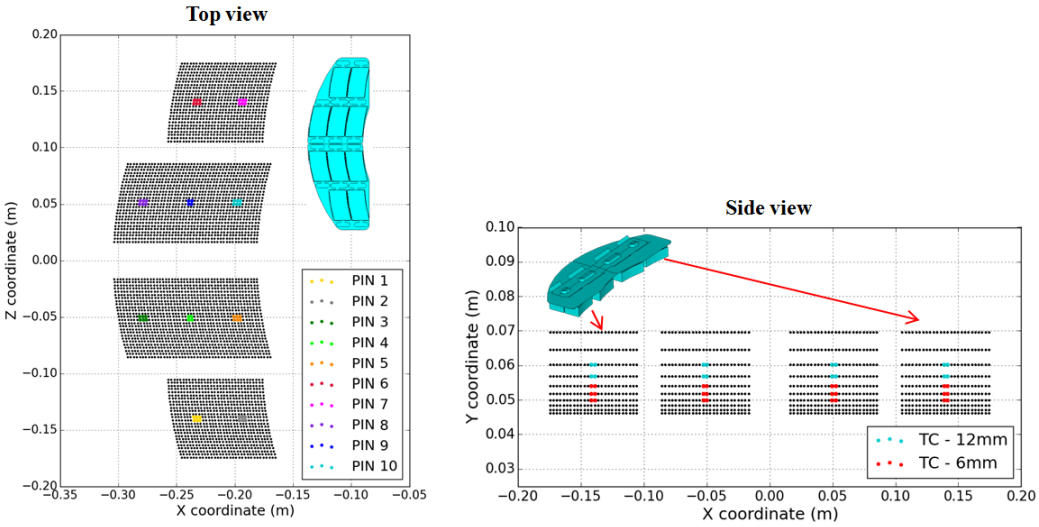

Figure 26: Example of the numerical selected nodes corresponding to experimental thermocouple locations.

The comparison of thermocouple temperatures obtained in the brake pads at the front and rear surfaces is transferred on the right side of figures 27 and 28. The pins located at the contact leading edge exhibit the highest temperature due to the angular engagement effect. Similar results are observed along the braking path by comparing the simulation results (continue lines on the figures) with the experimental results. On the rear side, the heat build-up within the pads seems is more concentrated on the outer radius. The responses from the model have the same tendency with values of the same order of magnitude. Nevertheless, some differences remain on pins n^o1 and 2, especially at the beginning of the test (t$\lesssim$20s). Experimentally, the contact is strongly localized on the front of the seal. The initial positioning of the pad must be different from that of the model. Note that the signals from the pin thermocouples n^o5 and n^o10 were

lost during the test.

More generally, there is a significant asymmetry of the thermal response between the front and rear surfaces. Indeed, higher temperatures are obtained on back pad pins (around 100^oC) for experimental and numerical results. This can be explained by the behaviour of the disc which takes on a conical shape due to the thermomechanical loading.

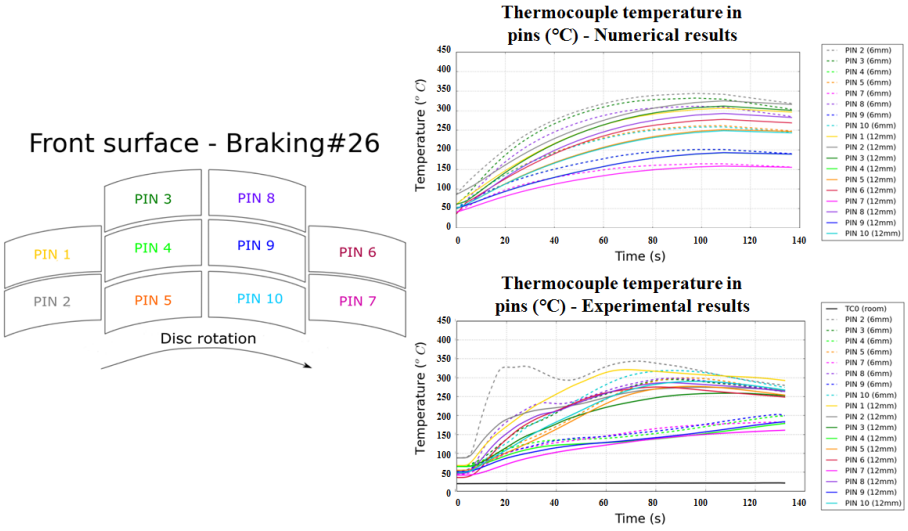

Figure 27: Comparison between numerical and experimental results of the brake pad thermocouples for the braking n^o26 - Front surface.

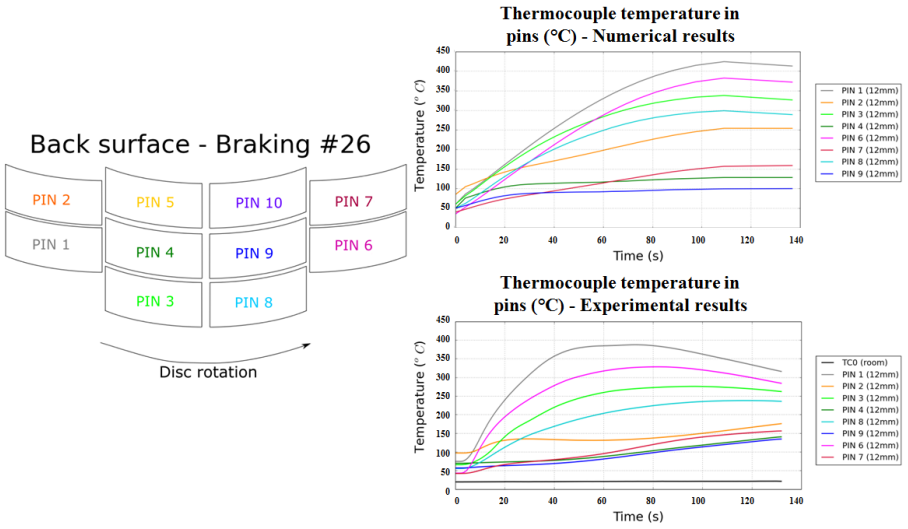

Figure 28: Comparison between numerical and experimental results of the brake pad thermocouples for the braking n^o26 - Back surface.

5. Proposition of a new brake pad design

As the numerical model has been validated in the previous sections, it is then possible to consider the assumptions made in order to propose a new design of brake pad. This new configuration is shown in figure 29.

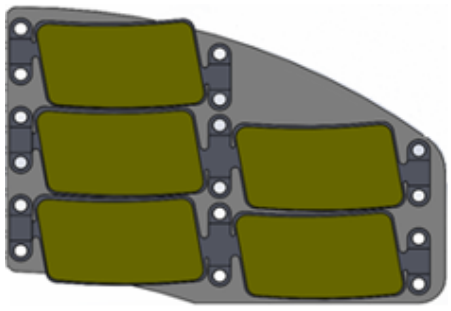

Figure 29: New configuration of the braking pad

The same simulation is performed and the results are shown in figure 30 in terms of temperature.

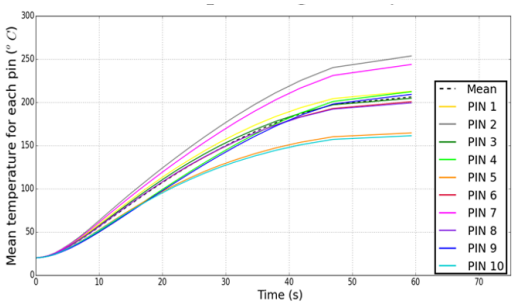

Figure 30: Evolution of the temperature for each pins with the improved brake pad at the rear face

By comparing the temperature level at the same points as before, it appears that on each pin there is a significant decrease. This temperature drop therefore has an impact on wear. The wear evolution for the reference configuration and the improved configuration are described in figure 31.

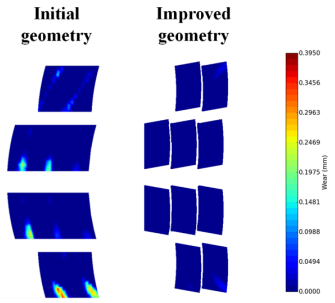

Figure 31: Wear at the end of the simulation for reference configuration (left-side) and the new configuration (right-side)

It turns out that the new configuration allows a better temperature distribution on all the pins and thus reduces wear by 40%.

6. Conclusion

This work focuses on the thermomechanical evolution of a HST type braking system from a numerical and experimental point of view. To evaluate the representativeness of a braking simulation, the thermal and mechanical properties

of the friction pad have been characterized at different temperature levels. The mechanical behaviour is obtained with a hot compressibility test using the DIC. Thermal properties are deduced from LFA and dilatometer tests. The thermomechanical behaviour has been identified and integrated into a UMAT to simulate the complete brake system. This model is based on a 1:1 experimental test bench of the industrial partner on which tests have also been carried out. In order to compare the experimental and numerical results, a dedicated braking campaign has been carried out using enhanced instrumentation. A wear pattern is also considered as a function of pressure and temperature at least inspired by the experimental test. The comparison between model and experiment showed that the overall behaviour of the brake pads and the thermal response of the disc is similar to that of the numerical model. Indeed, the number and location of thermal gradients observed on the disc are similar to those observed by infrared acquisitions. Similarly, the thermocouple responses, whether for the disc or the brake pads, give a similar thermal response between the simulation and the experiment. The methodology is therefore relevant to simulate the selected braking (number n^o26). Nevertheless, the n^o26 brake and previous ones are relatively low energy braking. In other words, the material evolves but slightly.

A mechanical characterization of the material at the end of the test protocol was performed and exhibited significant transformations in depth. Thereafter, it would be necessary to be able to take this evolution into account in order to be able to treat braking with a higher energy. On this type of braking, especially when it is very energetic, a thermal gradient appears along the circumference of the disc (hot spotting). The model will therefore have to be able to simulate this kind of phenomenon in the same way as [26, 27].

Acknowledgments

The present research work was carried out within the GLGV project backed by SNCF, Flertex, the LaMcube, and the organization ADEME. The authors grate-fully acknowledge the support of these institutions.

[1] Dufrénoy, P., 2004, *Two/three dimensional hybrid model of the thermomechanical behaviour of a disc braking system* J. of Mechanical Engineering Science. Proc. Instn Mech. Engrs Part F 218 17-30.

[2] Gao, C.H., Huang, J.M., Lin, X.Z., Tang Guo, X. S., Aziz, H., Schmidt, NI., 2006, *Stress Analysis of Thermal Fatigue Fracture of Brake Disks Based on Thermomechanical Coupling*, Journal of Tribology, vol. 129, issue 3, pp. 536-543.

[3] Kato, K., 2000, *Wear in relation to friction: a review*, Wear, vol:241(2), pp: 151-157.

[4] Rossmanith, H.P., Loibnegger, F., Huber, R., Rossmanith, H.P., Loibnegger, F., Huber, R, 2006. *Thermomechanical fatigue fracture due to repeated braking of railway wheels.* Materials Science, vol. 42(4), pp. 466-475.

[5] Bijwe, J., Majumdar, N., Satapathy, BK., 2005. *Influence of modified phenolic resins on the fade and recovery behavior of friction materials*, Wear, vol. 259(7), pp.1068-1078.

[6] Kao, TK., Richmond, JW., Douarre, A., 2000. *Brake disc hot spotting and thermal judder: an experimental and finite element study*, International Journal of Vehicle Design, Vol. 23(3), pp. 276-296.

[7] Wong, J. , 2000. *Analyse de l'endommagement par fatigue thermique et modélisation du comportement thermomécanique de couples disques-garnitures de type TGV*, PhD thesis.

[8] AbuBakar, AR., Ouyang, H., 2008. *Wear prediction of friction material and brake squeal using the finite element method*, Wear, Vol. 264, pp. 1069-1076.

[9] Panier, S., Dufrénoy, P., Weichert, D., 2004. *An experimental investigation of hot spots in railway disc brakes*, Wear, Vol. 256, pp. 764-773.

[10] Kim, DJ., Lee, YM, Park, JS, Seok, CS, 2008. *Thermal stress analysis for a disk brake of railway vehicles with consideration of the pressure distribution*

on a frictional surface, Materials Science and Engineering: A, Vol. 483, pp. 456-459.

[11] Söderberg, A., Andersson, 2009. *Simulation of wear and contact pressure distribution at the pad-to-rotor interface in a disc brake using general purpose finite element analysis software*, Wear, Vol. 267, pp. 2243-2251.

[12] Belhocine, A., Bouchetara, M., 2013. *Investigation of temperature and thermal stress in ventilated disc brake based on 3D thermomechanical coupling model*, Ain Shams Engineering Journal, Vol. 4, pp. 475-483.

[13] Grzes, P., 2017. *Simulation of braking for a pad-disc system at temperature-dependent coefficient of friction and properties of materials.* Eurobrake 2017, Dresden (Germany).

[14] Wegmann, E., Stenkamp, A., Dohle, A., *Relation between compressibility and viscoelastic material properties of a brake pad,* tech. rep., SAE Technical Paper, 2009

[15] Mann, R., Magnier, V., Brunel, JF., Brunel, F., Dufrénoy, P., Henrion, M., 2017. *Relation between mechanical behavior and microstructure of a sintered material for braking application*, Wear, Vol. 386-387, pp. 1-16.

[16] Hild, F., Roux, S., 2006. *Digital image correlation: from displacement measurement to identification of elastic properties–a review,* Strain, vol. 42, no. 2, 605 pp. 69–80.

[17] Réthoré, J., Besnard, G., Vivier, G., Hild, F., Roux, S., 2008. *Experimental investigation of localized phenomena using digital image correlation,* Philosophical Magazine, vol. 88, no. 28-29, pp. 3339-3355.

[18] Avril, S., Bonnet, A., Bretelle, A.S., Grédiac, M., Hild, F., Ienny, P., Latourte, F., Lemosse, D., Pagano, S., Pagnacco, E., Pierron, F., 2008. *Overview of Identification Methods of Mechanical Parameters Based on Full-field Measurements*, Experimental Mechanics, Vol. 48, pp. 381.

[YADICS] YADICS, Software: *http://yadics.univ-lille1.fr/wordpress/*.

[20] Parker, WJ, Jenkins, RJ, Butler, CP, Abbott, GL, 1961. *Flash method of determining thermal diffusivity, heat capacity, and thermal conductivity*, Journal of applied physics, Vol. 32(9), pp. 1679-1684.

[Ansys] Ansys V16. 2016, SAS IP, Inc.

[22] Simo, JC, Hughes, TJR, 1987. *General return mapping algorithms for rate-independent plasticity*, Constitutive laws for engineering materials: theory and applications, Vol. 1, pp. 221-232.

[UIC] International union of railway (UIC): http://www.uic.org/.

[24] Vernotte, 1956. *Calcul numérique, calcul physique, application à la thermocinétique*, Vol. 319.

[25] Archard, JF., 1959. *The temperature of rubbing surfaces*, Wear, Vol. 2, pp. 438-455.

[26] Tang, J., Bryant, D., Qi, H.S., 2016. *A 3d finite element simulation of ventilated brake disc hot spotting.* In Eurobrake technical paper EB-2016-SVM-025.

[27] Panier, S., 2002. *Étude théorique et expérimentale des points chauds dans les organes de friction : application au freinage ferroviaire.* PhD thesis passée à l'USTL.